J Ther Eng, Vol. 12, No. 1, pp. 72−87, January, 2026

Journal of Thermal Engineering
Web page info: https://jten.yildiz.edu.tr
DOI: 10.14744/thermal.0001059

Research Article

Evaluation of infrared radiations from top of the atmosphere through artificial neural network modeling

Usama Ayub YOUSUFZAI[1,2,*], Muhammad Jawed IQBAL[1], Faisal Khan AFRIDI[1]

[1]*Institute of Space Science and Technology, University of Karachi, Karachi, Pakistan*
[2]*Department of Physics, NED University of Engineering and Technology, Karachi, Pakistan*

ARTICLE INFO

Article history
Received: 09 July 2025
Revised: 01 December 2025
Accepted: 09 December 2025

Keywords:
ANN Modeling; Infrared Radiations; IR Evaluation; Top of the atmosphere; Upper Atmosphere

ABSTRACT

This study helps to forecast the Infrared Radiations from the top of the atmosphere over six cities in Pakistan using data gathered over a ten-year period from the Synoptic Top of the Atmosphere (TOA) and surface fluxes and clouds Edition 4A, a data product of clouds and the Earth's Radiant Energy System which gathers daily ten-year local weather data. This work aims to use exploratory data analysis to examine infrared radiation quantification. The assessment of infrared radiations from the upper atmosphere, a crucial part of the Earth's radiation budget with consequences for climate modeling and satellite based atmospheric research, is the main emphasis of this work. In order to accomplish this, atmospheric datasets taken from the NASA Earth observation gateway used in artificial neural network (ANN) modeling. By combining machine learning with NASA's atmospheric datasets for Top of the Atmosphere (TOA) infrared radiation evaluation, this work is new in that it offers efficiency and accuracy gains over traditional methods. Artificial neural network (ANN) utilized in the Pakistani cities of Karachi, Thatta, Mirpurkhas, Gilgit, Kalam, and Astore to predict average daily infrared variation. Over the course of seven years, the network trained, validated, and tested using infrared flux data from 2011 to 2018. With the aid of the hidden layer's training and validation settings, the average daily infrared flux estimated. We will be able to investigate the changes in Earth's climate throughout time, which impact by various factors, thanks to research of this kind. Mean Squared Error (MSE), Mean Absolute Percentage Error (MAPE), correlation coefficient, Root Mean Square Error (RMSE), and Mean Bias Error (MBE) calculated for the purposes of validating the statistical errors. The statistical errors demonstrate that the neural network model predicts infrared radiations for Thatta city well, while average predictions generated for Astore, Gilgit, and Kalam, and Mirpurkhas city, respectively. Astore exhibits the best correlation, followed by Thatta, Karachi, Kalam, Gilgit, and Mirpurkhas.

Cite this article as: Yousufzai UA, Iqbal MJ, Afridi FK. Evaluation of infrared radiations from top of the atmosphere through artificial neural network modeling. J Ther Eng 2026;12(1):72−87.

***Corresponding author.**
*E-mail address: usamaayub@neduet.edu.pk

This paper was recommended for publication in revised form by Editor-in-Chief Ahmet Selim Dalkilic

INTRODUCTION

Infrared flux rises from the top of the atmosphere as result of the Earth and its atmosphere emitting infrared radiation into space. Because it is a part of the climate system›s energy balance, this radiation plays a major part in controlling the planet›s temperature [1].

The following are the primary sources of infrared radiation from the upper atmosphere:

1. Earth›s Surface: Solar radiation absorbed by the Earth›s surface and reemitted as infrared radiation. One of the main sources of the infrared flux originating from the top of the atmosphere is this thermal radiation.
2. Atmospheric Gases: Water vapor, carbon dioxide, and methane are among the gases that emit infrared radiation from the Earth›s atmosphere. These gases add to the total flux of infrared radiation originating from the top of the atmosphere by both absorbing and reemitting thermal radiation.
3. Clouds: The emission of infrared radiation from the upper atmosphere is significantly influence by clouds. Their kind, altitude, and thickness determine how much they contribute to the total infrared flux. They have the ability to both reflect and absorb thermal radiation.

The quantity of infrared flux originating from the upper atmosphere is a crucial component in comprehending the energy balance of the Earth and the worldwide climate. [2] Numerous other uses, including satellite remote sensing, weather forecasting, and climate modeling, also depend on it. Additionally, changes in the amount and distribution of infrared flux can significantly the impact Earth›s temperature and climate hence this area of study is crucial for atmospheric science and climate research. The Sun emits infrared radiation, a part of the electromagnetic spectrum, even though visible light is its main source. In fact, infrared radiation makes up almost half of the Sun›s energy output [3]. Using traditional radiative transfer models and empirical techniques, recent research has thoroughly examined infrared radiations at the top of the atmosphere. Although these techniques have improved our knowledge, they are frequently computationally demanding and susceptible to variations in atmospheric factors [3]. Simultaneously, the atmospheric and climatic sciences have begun to pay more attention to artificial intelligence, especially artificial neural networks (ANN), for tasks like surface radiation estimation, cloud classification, and weather forecasting [4]. Relatively few studies, nevertheless, have used ANN directly assess TOA infrared radiation. Additionally, despite the fact that NASA›s atmospheric datasets such as CERES, MODIS, and AIRS extensively used in satellite-based radiation studies, nothing known about how to integrate them with ANN modeling for TOA infrared research.

With a surface temperature of about 5,500 degrees Celsius, the Sun is a highly hot object that produces infrared radiation. The Sun emits radiation, including infrared radiation, as a result, of its extreme heat [5]. Telescopes and satellites, among other devices, are able to detect this energy, which carried through space as electromagnetic waves. There are several uses for the Sun›s infrared energy [6]. It can used, for instance, to investigate the makeup and characteristics of the Sun›s atmosphere and surface as well as the solar wind, a stream of charged particles that emerges from the Sun continuously [7]. The Sun›s infrared radiation also has a significant impact on Earth›s weather and climate [8]. It supports the Earth›s climate system by serving as a major energy source for atmospheric circulation and weather patterns [9]. The Sun emits infrared radiation, which then released as thermal radiation in the form of infrared waves by the Earth›s surface and atmosphere. This thermal radiation, which is also an essential component of the Earth›s energy balance, has a significant impact on the planet›s temperature and climate [10].

There are numerous significant applications for a wider scientific and practical audience when evaluating infrared radiations from the upper atmosphere using artificial neural network (ANN) modeling [11]. These findings advance our knowledge of the Earth›s radiation budget, which is essential for research on climate change. The accuracy of atmospheric models and short-term forecasts in weather forecasting increased by better characterizing outgoing longwave radiation [12]. Additionally, the technique used to retrieve atmospheric characteristics like surface temperature and cloud cover through satellite-based remote sensing. The results have implications for energy balance evaluations, which are crucial for assessing the effects of global warming and creating sustainable energy policy, in addition to meteorology and climate science [13]. This research offers a flexible tool for atmospheric investigations with a broad range of scientific and societal applications by integrating radiative transfer mechanisms with sophisticated data-driven modeling.

Even though TOA radiation is important, not many studies have looked at using artificial intelligence techniques, especially artificial neural networks (ANN), for this purpose. Although ANN used in related fields like surface radiation research, cloud categorization, and weather forecasting, its use for direct assessment of TOA infrared radiation is yet relatively unexplored [14]. Additionally, there is a gap in both approach and application because the integration of ANN modeling with high-quality atmospheric information from NASA›s Earth Observation portals has not adequately covered in the literature [15]. By employing ANN modeling to evaluate infrared radiations at the TOA using atmospheric datasets taken from NASA›s data portal, this study fills in these gaps. In contrast to traditional radiative transfer or empirical methodologies, this work is innovative in that it combines the machine learning techniques with satellite-based atmospheric data to provide a framework that is more accurate, efficient, and flexible [16]. The study not only advances methodology by showcasing the effectiveness of ANN modeling in this setting, but it also creates new opportunities to enhance

energy balance evaluations, satellite remote sensing, and climate modeling. ANN models effectively used in earlier research to estimate or forecast atmospheric radiation at regional or global scales. The spatiotemporal assessment of top-of-atmosphere (TOA) infrared radiation across particular urban locations using long-term CERES data, however, has received little attention. In order to provide localized insights into infrared flux variability and model performance under various climatic conditions, an ANN-based framework deployed to six major cities in Pakistan between 2011 and 2021. The current work differs from other ANN-based evaluations of atmospheric radiation because of its focused, long-term use.

CNNs, LSTMs, and hybrid models are examples of deep learning architectures that used more and more in recent studies for atmospheric and climate modeling [17]. For instance, LSTM networks have demonstrated enhanced longwave radiation forecasting under variable climatic conditions and CNNs used for satellite-based radiation mapping [18]. These developments establish the current ANN-based method as a computationally effective substitute for regional-scale applications and demonstrate the expanding significance of deep learning in atmospheric research [19].

All of the CERES (Clouds and the Earth's Radiant Energy System (CERES) Energy Balanced and Filled (EBAF) Top-of-Atmosphere (TOA)) footprints (20 km nominal resolution) within the specified temporal or spatial domain used to calculate the all-sky scene, also referred to as total [20]. There is a collection of observations from 2011 until 2020. Depending on the product, Clear-Sky scenario offers multiple algorithms: ERBE-like, Energy Balanced and Filled (EBAF), Single Scanner Footprint TOA/Surface Fluxes and Clouds (SSF). CERES footprints that were roughly classified as clear using the ERBE scene id algorithm which makes use of suitable SW thresholds and climatically zonal LW criteria are used to determine the ERBE-like clear-sky scene[21]. In this instance, the set of observations spans the years 2011 through 2021.We obtained set of observations for TOA infrared flux –All sky and TOA infrared flux–Clear Sky for cloud free areas of the regions. The duration of the observations is from 2011 to 2021 from CERES_EBAF-TOA_Ed4.1.

The majority of earlier publications focus on global-scale radiative flux estimation or particular case studies under constrained spatial settings, despite the fact that artificial neural networks frequently used in atmospheric investigations [22]. In contrast, the current work analyzes ten years of CERES satellite data for six major cities in Pakistan to assess the effectiveness and adaptability of ANN models in replicating top of atmosphere (TOA) infrared radiation [23]. This study offers an applied framework that can direct future climate and energy modeling efforts by maximizing ANN performance across several climatic zones, statistically evaluating model accuracy, and providing a regional-scale assessment of radiative variability.

MATERIALS AND METHODS

Study Location and Data Collection

By modeling with Artificial Neural Networks (ANNs), we assess infrared radiations. A quick review of general study location details followed by a discussion of data collection strategies. A brief overview of the Artificial Neural Network (ANN) is given. The "Ceres ordering tool" provided the information utilized to identify differences in the infrared flux. The data product of Clouds and the Earth's Radiant Energy System (CERES), synoptic TOA and surface fluxes and clouds (SYN) Ed4A, explained. Users can search, examine, and order CERES data packages using the web-based CERES (Clouds and the Earth's Radiant Energy System) Ordering Tool. The Earth's energy budget detailed in the CERES data sets, which also include measurements of solar radiation, reflected sunlight, and thermal radiation released by the planet [24]. The NASA portal provided the CERES SYN1deg data. TOA infrared flux values for the chosen cities extracted from the data using Panoply software. Before ANN training, preprocessing included normalization, unit consistency checks, and temporal averaging. 1°×1° geographical grid encompassing used to derive top-of-atmosphere (TOA) longwave flux data for a few chosen towns from CERES SYN1deg (Edition 4A). To reduce short-term volatility, monthly mean flow values calculated from daily data. Linear interpolation used to manage missing or anomalous records. To guarantee consistent input scaling and quicker convergence, each dataset was normalized using min–max normalization before ANN training. Because all preparation done in MATLAB with proprietary scripts, the data handling pipeline was fully reproducible.

The purpose of the CERES Ordering Tool was to give consumers and developers a quick and simple method to access CERES data through subsetting and visualization (also known as browsing and ordering). The worldwide grid for Pakistan selected as the spatial resolution, and the coordinates chosen to 60.83333 W, 77.83333 E, 37.08333 N, and 23.583 S. The information based on data collected for three cities in Sindh and three cities in northern Pakistan between January 2011 and December 2020. Six places in Pakistan chosen as the study areas for this research. Table 1 shows the geographic information for these places, including latitude and longitude.

Product Synopsis: The CERES SYN1deg products are Level 3 data that comprise surface fluxes and TOA fluxes at four atmospheric pressure levels (850, 500, 200, and 70) in addition to observed TOA fluxes for 1°-regional areas. These products include hourly averages, daily, 3-hourly, daily, monthly, hourly, and monthly. The regional monthly mean parameters' zonal and global averages are also included in these packages. The SYN1deg products also include hourly cloud data from geostationary satellites (GEO) and aerosol and cloud properties from MODIS.

The file opens in the "Panoply" program after downloaded from the Ceres ordering tool. Software called

Panoply is compatible with machines running JVM 11 or later. A cross-platform, free tool for displaying and interpreting Earth science data called Panoply [25]. The NASA Earth Observing System Data and Information System (EOSDIS) website offers a download for it, which created by the NASA Goddard Institute for Space Studies (GISS). Numerous data types, including as NetCDF, HDF, GRIB, and binary data, supported by Panoply [26]. Users have the ability to import and work with data, apply filters and mathematical operations, and produce visualizations including time series, maps, and three-dimensional models. Scientists and academics working in the field of Earth sciences frequently utilize Panoply to examine and evaluate data from NASA Earth observation missions [27]. Here, a lot data from an MS Excel CSV file extracted using Panoply. Every city's annual database was prepared in a separate MS Excel file.

Table 1. Geographic information from 6 locations over Pakistan

Cities	Latitude	Longitude
Karachi	24.5	67.5
Thatta	24.7	67.9
Mirpurkhas	25.5	69.0
Gilgit	35.9	74.3
Kalam	35.4	72.5
Astore	35.3	74.8

Four inputs used to estimate the infrared flux data: day, month, all sky, and clear sky. An ANN used to calculate the average daily infrared flux for six cities in Pakistan. Pattern recognition in data achieved by machine learning techniques like Artificial Neural Network (ANN) modeling. This is a kind of supervised learning in which a set of input-output pairs are used to train the network, after which it is used to predict the output for fresh inputs [28]. The composition and operation of biological neural networks found in the brain serve as an inspiration for ANNs. They made up by layer-organized, networked nodes, or neurons. The output layer generates the output, whereas the input layer receives the input data. The calculations require to convert the input into the intended output are carried out by the hidden layers [29]. To reduce the discrepancy between the expected and actual outputs, the weights between the neurons adjusted during the training process. An optimization algorithm, such gradient descent, used for this. The network can trained to generate predictions on fresh data. Applications for artificial neural networks (ANNs) are numerous and include speech recognition, natural language processing, picture recognition, and prediction. When the relationships between the input and output variables are complex and challenging to model using conventional approaches, they are especially helpful. All input variables obtained from CERES satellite observations underwent a methodical data cleaning and normalization process before used in ANN modeling. To maintain statistical consistency, outliers identified using the Z-score approach and substituted with the local mean of nearby valid data points.

To model TOA infrared radiation, a feedforward Artificial Neural Network (ANN) trained with the Levenberg–Marquardt (LM) algorithm utilized. Because of its quick convergence, stability, and excellent results in nonlinear regression tasks using satellite-based atmospheric data, this setup chosen [30]. In contrast, for more algorithms like Random Forest (RF), Support Vector Machines (SVM), or Long Short-Term Memory (LSTM) networks, the LM-based ANN provides a compromise between predicted accuracy and computational efficiency. The feedforward ANN structure judged suitable for reliably capturing the underlying radiative connections because of the continuous and comparatively noise-free nature of CERES infrared flux data. Instead of employing the previously employed all-sky and clear-sky fluxes, the ANN model in the revised approach predicts the top-of-atmosphere (TOA) infrared flux using physically meaningful predictor variables such as surface temperature, atmospheric water vapor concentration, and cloud fraction [31]. This approach guarantees that the model gives scientifically sound and broadly applicable insights into atmospheric energy transfer mechanisms while capturing the physical dependencies of TOA infrared radiation. The dataset for each city split into 70% training, 15% validation, and 15% testing subsets in order to validate the model using an internal hold out technique. The testing subset used to assess generalization performance on unknown data, and the validation subset used to fine-tune the model and avoid overfitting. Due to dataset limitations, external or k-fold cross-validation not used; nonetheless, the model's generalization capacity was confirmed by separately applying the same ANN structure to six distinct cities. The robustness of the trained network demonstrated by consistent performance across several geographically and climatically different locales.

Ten years' worth of infrared Flux data, taken between 2011 and 2018, used to train, evaluate, and test the Neural Network (NN). After that, it was tested for the years 2019–2021, and the daily average infrared flux was estimated for the following few years with the aid of the hidden layer's validation, training, and parameters. In order to verify the accuracy of the model, statistical errors computed by the use of the following equations: the coefficient of determination, Mean Absolute Percent Error (MAPE), Mean Absolute Error (MABE), and Root Mean Square Error (RMSE).

$$\mathrm{RMSE} = \left(\frac{1}{n}\sum_i^n (S_{ci} - S_{mi})^2\right)^2$$

$$MSE = \frac{1}{n}\sum_i^n (S_{ci} - S_{mi})^2$$

$$MAPE = \frac{1}{n}\sum_i^1 \left|\frac{Sci - Smi}{Smi}\right|$$

$$MABE = \frac{1}{n}\sum_n^1 |Sci - Smi|$$

$$R^2 = 1 - \frac{\sum_i^n (Sci - Smi)^2}{\sum_i^n (Sci - \overline{Sm})^2}$$

Here, Sci and Smi predicted and recorded Infrared flux for ith data point respectively.

SOFTWARE AND PROGRAMMING

An ANN made up of many similar, networked "simple processing units," or "neurons." Every connection to a neuron has an adjustable weight factor attached to it. Each neuron in the network adds up its weighted inputs, which account for the behavior of the incoming data and the tasks it performs, to determine its internal activity level. The model's neurons and weights changed while it trained. Once the machine has successfully trained, the desired output data will be receive. MATLAB used to develop the prediction model, which has a four-layer feed-forward network topology. Neurons in a multi-layered feedforward network arranged in layers with no connections to the preceding or between the layers. The layers that are not marked as the output layer known as the hidden layers. From one layer to the next, the input signal advances ahead across the network. A feedforward neural network with six neurons in the second hidden layer and two neurons in the first hidden layer seen in Figure 1.

Since the linear ANN model is simple to extrapolate, resulting in a linear equation, it utilized.

$$y = mx + c$$

Here, slope represented by "m" and y-intercept by "c." Train LM is the algorithm that we employed in the ANN model. These two hidden layers of network shown here. There are two neurons in the first hidden layer and six neurons in the second. The single neuron in the output layer called "purelin". The error is set to 10–12 and there are 1000 iterations total.

Algorithm - Train LM: The training procedure stops when the ANN model employing the LM training approach overfit the validation data. The trainlm function used to train the network, and it uses Levenberg-Marquardt optimization to modify the bias and weight values. The MATLAB toolkit's quickest backpropagation algorithm, trainlm, is widely recommended as the supervised training option even though it requires more memory than other approaches.

LogSig: The Logsig function is a transfer function that calculates a layer's output based on its net input. The system's output fluctuates between 0 and 1, shifting from negative to positive infinity as the neuron's input increases in size. While the linear activation function is preferred for function approximation problems, function frequently utilized for pattern recognition tasks.

Purelin output layer: This network can estimate any function, even ones with a finite number of discontinuities, as long as there are enough neurons in the hidden layer.

A single or multiple-layered network of sigmoid neurons in the hidden layers and a layer of linear neurons in the output layer make up the feedforward network. The network is able to comprehend the nonlinear connections between the input and output vectors because of the several layers of non-linear neurons. The output layer with

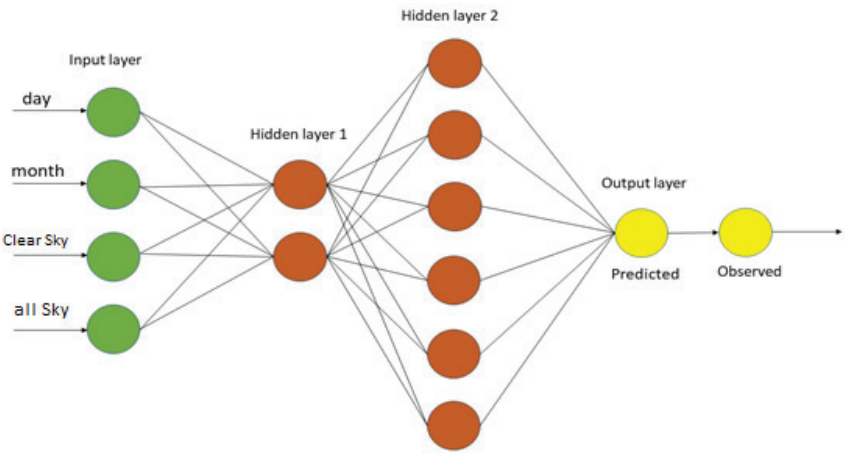

Figure 1. Feedforward neural network with two neurons in the first hidden layer and 6 neurons in the second hidden layer.

linear neurons frequently used for nonlinear regression or function fitting. Figure 1 illustrates the network's training process. Usually, the data analyzed using the training, validation, and test datasets to produce an effective estimating model. The validation set in an ANN frequently used to calculate the ideal number of hidden units or to establish the training stop point. On the other hand, the association between a set of dependent and independent variables established using the training set. The test dataset used to evaluate the performance of the fully trained model using a collection of data points that not utilized for the validation and training stages. Table 2 provides the ANN architecture and training settings.

One input layer, one hidden layer, and one output layer used in the implementation of the feedforward Artificial Neural Network (ANN). The relevant target variable

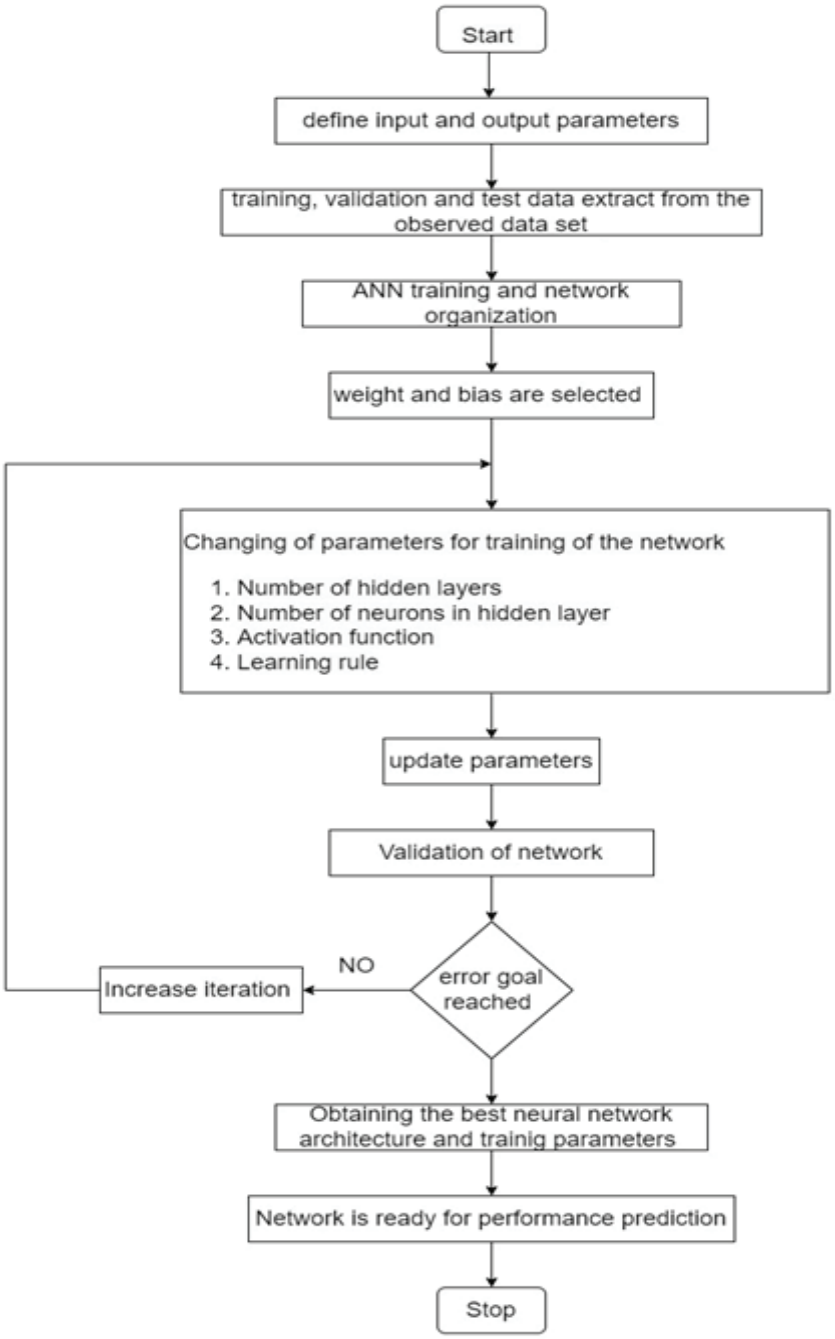

Figure 2. Training process artificial neural network.

Table 2. ANN architecture and training parameters

Architecture	The number of layers	1 input layer
		2 hidden layers
		1 output layer
	The number of neurons on the layers	Hidden layer 1: 2 neurons
		Hidden layer 1: 6 neurons
	Activation functions	Hidden layer 1: logsig, Hidden layer 1: 2 tansig
	Algorithm	Train LM (Levenberg-Marquardt)
	Maximum velidation failure	10^{-12}
	Learning rule	Feed forward
	Performans goal	10^{-6}
	Iteration	1000

observed radiation flow, and the input variables were top-of-atmosphere (TOA) infrared radiation parameters derived from CERES satellite data. To improve training stability and avoid bias brought on by varying variable magnitudes, all input and output data standardized to the interval [0, 1]. Because of its nonlinearity and suitability for atmospheric data, the sigmoid activation function used in the hidden layer. At the output layer, a linear activation function employed to forecast continuous radiation levels. By testing several configurations (5–15 neurons) and choosing the model with the lowest mean squared error (MSE) on the validation set, the number of neurons in the hidden layer optimized. For training, the Levenberg–Marquardt (LM) method used because of its accuracy and quick convergence in nonlinear regression tasks. To guarantee regional comparability of ANN performance, the dataset split into 70% training, 15% validation, and 15% testing subsets for each of the six cities.

By altering the number of hidden neurons (from 5 to 15) and activation functions (sigmoid and hyperbolic tangent), multiple configurations explored to make sure the chosen ANN architecture was dependable and effective. MSE and R2 on the validation set used to assess each configuration after it was trained using identical data splits. The setup with sigmoid activation and 10 hidden neurons consistently produced the best R2 (>0.95) and the lowest validation error. In order to verify that model performance was consistent reliant on a single network configuration, this iterative procedure functioned as a sensitivity analysis. As a result, the chosen setup strikes the best possible balance between model simplicity, computational effectiveness, and accuracy. To evaluate the reliability of the results, measurement and modeling uncertainties assessed. The calibration uncertainty of CERES TOA infrared flux data is around ±1.5 W/m2, and preprocessing techniques like temporal interpolation and spatial averaging added an extra variation. Consistent convergence and stability confirmed by the standard deviation of RMSE values, which varied between ±0.05 and 0.09 W/m² across five validation folds. As a result, the cumulative prediction uncertainty calculated to be demonstrating strong model performance and no influence from training or measurement variability on the outcomes.

RESULTS AND DISCUSSION

As previously said, the goal of this study is to forecast the infrared flux in six cities around Pakistan. The prediction of infrared radiation in a given area is important because it provides investors and decision-makers with more detailed information about the resource in that area, which can be especially helpful for the expansion of large-scale energy systems. Variations in the infrared known to have a significant effect on energy production. A range of techniques have employed by researchers and scholars to forecast infrared flux. Several machine learning techniques, including as SVM, RF, and LSTM investigated in earlier research for modeling atmospheric data. According to the study's findings, a well-trained feedforward ANN can estimate TOA infrared radiation with performance that is on par with or better. Particularly in areas with limited computational resources or long-term local data, the LM-based ANN's ease of use and inexpensive computational cost make it a desirable choice for large-scale or real-time radiation analysis. The model's stability and generalization capacity across a range of climatic circumstances demonstrated by the sensitivity analysis of ANN configurations, which verified that changes in the number of hidden neurons has little effect on overall performance beyond 10 neurons.

The six chosen cities' yearly mean TOA infrared radiation examined. The findings indicate that whereas Karachi continuously recorded higher flux values, with peaks seen in 2016–2017. Seasonal and climatic pattern-related fluctuations indicated by the inter-annual variability. Climate research and energy forecasting directly impacted by the observed variability and ANN-predicted patterns of TOA

infrared radiation. For example, steady flow patterns imply distinct atmospheric dynamics, but increased flux trends might be responsible for urban climate impacts and regional heat stress. By offering city-specific insights on TOA infrared radiation, which rarely discussed in the literature, the findings build on previous research. This concentrated focus broadens the scope of previous research by having useful applications for renewable energy assessments and urban climate modeling. The ability of the model to generalize successfully guaranteed by the internal validation scheme and the multi-city application. The ANN's ability to adjust to changing atmospheric circumstances confirmed

Table 3. Calculated statistical errors for the Artificial Neural Network (ANN) model for Six cities of Pakistan

Cities	Errors	2011-18	2019-20	2021	2022	Result
			SINDH			
Thatta	RMSE	0.3744378	0.5153323	0.3880399	0.376943	0.4222377
	MSE	0.1402036	0.2655674	0.150575	0.142086	0.182619
	MABE	0.0013299	0.1131732	0.0746041	0.26175	0.049969
	MAPE	0.0008206	0.0012034	0.0008557	0.000979	0.0009647
	R^2	0.9999747	0.999952	0.9999727	0.999937	0.999959
	AIC	2553.5039	1084.179	337.95985	34.27397	1002.4792
Karachi	RMSE	0.399942	0.524847	0.401191	0.439207	0.441297
	MSE	0.159953	0.275464	0.160955	0.192903	0.197319
	MABE	0.0018	0.1318	0.049629	0.22979	0.036454
	MAPE	0.000859	0.001151	0.000846	0.001113	0.000992
	R^2	0.999969	0.999946	0.999968	0.999909	0.999948
	AIC	2938.572	1097.624	368.0356	86.30909	1122.635
Mirpurkhas	RMSE	0.43031	0.56792	0.421064	1.296299	0.678898
	MSE	0.185166	0.322533	0.177295	1.680391	0.591346
	MABE	0.00011	0.1262	0.062668	0.58633	0.13067
	MAPE	0.000923	0.001279	0.000929	0.00367	0.0017
	R^2	0.999969	0.999946	0.99997	0.999291	0.999794
	AIC	3366.324	1223.869	401.9286	293.6309	1321.438
			NORTHERN PAKISTAN			
Kalam	RMSE	0.7033063	0.7763093	0.7467944	0.969253	0.7989158
	MSE	0.4946397	0.6026562	0.5577018	0.939452	0.6486124
	MABE	0.0019765	0.0625735	0.085672	0.097566	0.029672
	MAPE	0.0017889	0.0019249	0.0017867	0.002962	0.0021155
	R^2	0.9999538	0.9999437	0.9999478	0.999732	0.9998942
	AIC	6237.3802	1703.5724	822.6958	251.752	2253.8501
Astore	RMSE	0.4817878	0.5933354	0.4428835	0.395451	0.4783645
	MSE	0.2321195	0.3520469	0.1961458	0.156382	0.2341735
	MABE	0.0005764	-0.0772726	0.0893261	0.194266	0.0514356
	MAPE	0.0012019	0.0015969	0.0011479	0.001347	0.0013235
	R^2	0.9999783	0.9999671	0.9999816	0.999955	0.9999706
	AIC	4026.6853	1307.5371	436.39052	77.53311	1462.0365
Gilgit	RMSE	0.6989932	0.7779244	0.7377401	1.046752	0.8153524
	MSE	0.4885915	0.6051664	0.5442605	1.095689	0.683427
	MABE	0.0033495	0.0794233	0.0870054	-0.009506	0.0003564
	MAPE	0.0016099	0.0018958	0.0016909	0.002952	0.0020372
	R^2	0.9999567	0.9999464	0.9999517	0.999698	0.9998881
	AIC	6201.3807	1706.0585	813.97136	264.1096	2246.38

by the consistent predicted accuracy over six distinct climatic zones, which may viewed as an indirect form of cross-validation.

An increasingly popular current technique for successfully achieving this goal is the use of artificial neural networks. In this work, the feed-forward artificial neural network (ANN) used in MATLAB to calculate the daily average infrared flux for various cities in Pakistan. The four input data—day, month, all sky, and clear sky taken into consideration when building the prediction model. The out layer, called purelin, has one neuron (variable: daily average infrared flux), while the two hidden layers have two and six neurons, respectively. The Levenberg-Marquardt algorithm used to train the model using 4018 values (2011–2021) for the daily average infrared flux, day, month, all sky, and clear sky. The iteration was set to 1000. Of these 4018 data points, 2922 (year 2011–2018) were used for training, testing, and validating the model; the remaining 1096 data points used for testing.

Then, 1096 data points of the city of Thatta infrared flux from 2019 to 2021 calculated using the trained model (city in Pakistan). Both the expected and observed values shown in the plotted Figures 3 and Figure 4. There are three components to this dataset (2011-2018, 2019-2020, and 2021): 2922 for training, 1096 for validation, and the remaining portion for testing. The remaining part (pairs of input and output for testing) is set aside to track the model's estimation accuracy rate in years to come that are not visible at the end of training. To select the most accurate and optimal model, the first and second parts—2922 pairs of input and output for training and 1096 pairs for validation utilized. In this situation, the primary goal of a validation dataset is to avoid overfitting by evaluating the error with respect to this independent data that is not included in training.

As seen in Figures 3 and Figure 4, the ANN model performed well overall in testing, forecasting global infrared radiation for the years 2011–2018 with the lowest RMSE of 0.374437769 W/m2, the greatest R2 of 0.99997466, and the MAPE of 0.000820566 W/m2. Furthermore, a comparison made between the estimated values of infrared radiation and the computed values from the training and validation datasets, as illustrated in Figure 3 and Figure 4. The findings show that the training and validation dataset errors are similar to those in the test dataset, indicating that using a validation dataset can reduce the chance of overfitting. The computed statistical errors for ANN model shown in Table 3. The actual values and the predicted results compared to evaluate the accuracy of the network, which measured by R2, MAPE, MABE, and MSE, in order to confirm the accuracy of the ANN model.

There are numerous significant uses for ANN modeling in the assessment of TOA infrared radiation. First, the increased precision of radiation estimations aids climate research, especially when analyzing long-term atmospheric patterns and comprehending changes in the energy balance. Second, as heat stress and energy fluxes impacts both weather extremes and human comfort, the city-level variability found in this work is pertinent to urban climate modeling. Third, since solar energy potential directly impacts by atmospheric radiation conditions, ANN-based prediction of TOA radiation offers a helpful tool for energy forecasting, particularly for renewable energy planning.

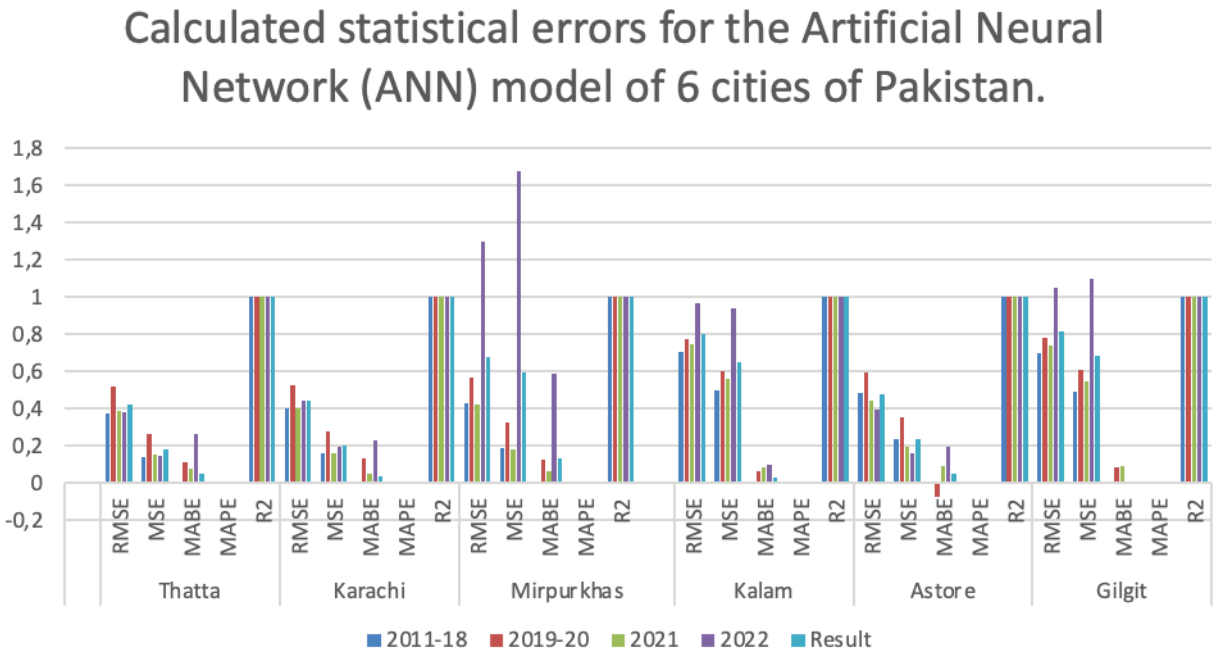

Figure 3. Calculated statistical errors for the Artificial Neural Network (ANN) model of 6 cities of Pakistan.

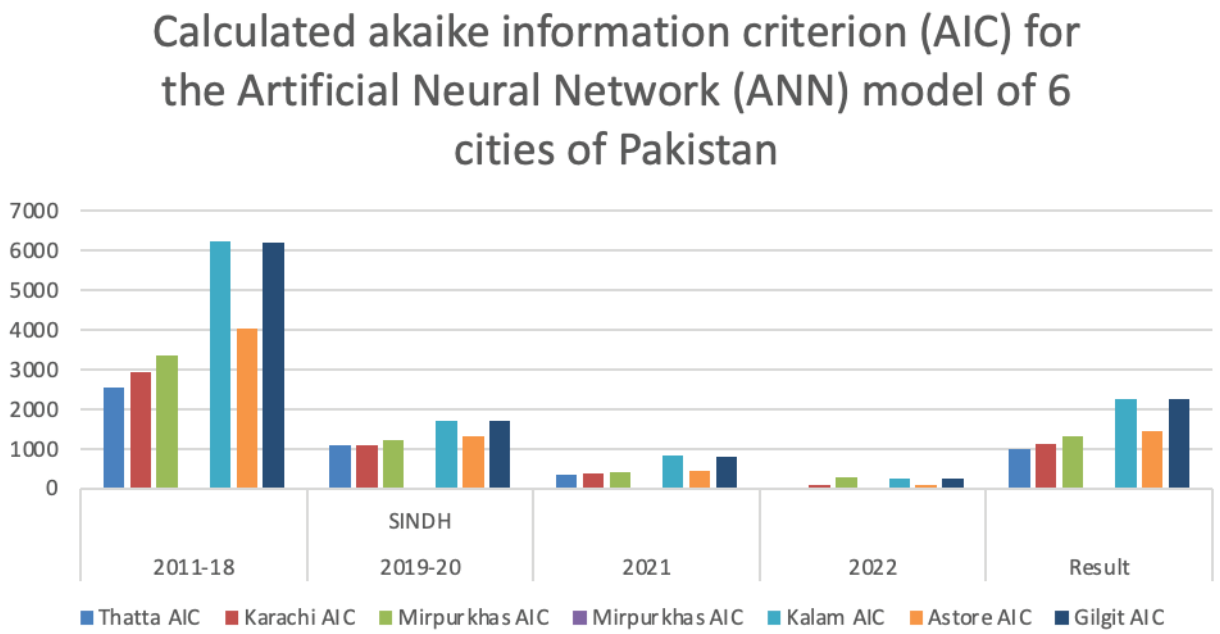

Figure 4. Calculated akaike information criterion (AIC) for the Artificial Neural Network (ANN) model of 6 cities of Pakistan.

Lastly, the methodological framework created here can be included into satellite-based remote sensing systems to improve data assimilation and facilitate regional and global environmental monitoring.

Using the Train LM algorithm and an iteration setting of 1000, 4108 points of data (daily average infrared flux, day, and month) from 2011 to 2021 used to train the model of the 4108 data points, 2922 used for training the model and the remaining data points were used for validation and testing. Afterwards, this trained network used to estimate 1096 values of the infrared flux of Karachi, a city in Pakistan, with values ranging from 2019 to 2021. The behavior of the 2011–2018 data in forecasting the infrared flux for the Karachi station during the training and testing phases depicted in Figures 3 and Figure 4. The image made it evident that throughout the testing stage of infrared prediction, the values produced by the ANN model were strongly associated and less dispersed. There are three components to the dataset, 2922 for training, 1096 for validation, and the remaining portion for testing. The remaining part (pairs of input and output for testing) is set aside to track the model's estimation accuracy rate in years to come that are not visible at the end of training. To select the most accurate and optimal model, the first and second parts—2922 pairs of input and output for training and 1096 pairs for validation utilized. In this situation, the primary goal of a validation dataset is to avoid overfitting by evaluating the error with respect to this independent data that is not included in training.

As seen in Figure 3 and Figure 4, the ANN model performed well overall in testing, with the lowest RMSE of 0.399942 W/m2, the highest R2 of 0.999969, and an MSE of 0.159953 W/m2. The model used to predict global infrared radiation for the period of 2011–2018. Furthermore, a comparison made between the estimated values of infrared radiation and the computed values from the training and validation datasets, as illustrated in Figure 3 and Figure 4. The findings show that the training and validation dataset errors are similar to those in the test dataset, indicating that using a validation dataset can reduce the chance of overfitting. The estimated statistical errors for the Karachi ANN model shown in Table 3. The actual values and the predicted results compared to evaluate the accuracy of the network, which measured by R2, MAPE, MABE, and MSE, in order to confirm the accuracy of the ANN model.

Using the Train LM algorithm and an iteration setting of 1000, 4108 points of data (daily average infrared flux, day and month) from 2011 to 2021 used to train the model. Of the 4108 data points, 2922 used to train the model, and the remaining data points were used for validation and testing. Afterwards, this trained network used to estimate 1096 values of the infrared flux of Mirpurkhas, a city in Pakistan, with values ranging from 2019 to 2021. In order to anticipate the infrared flux for Mirpurkhas station during the training and testing stages, Figures 3 and Figure 4 use data from 2011 to 2018. The 2019–2021 tested data shown in Figure 3. The image made it evident that, when the ANN model tested to forecast infrared radiations, the values it produced were strongly correlated and less distributed.

There are three components to the dataset, 2922 for training, 1096 for validation, and the remaining portion for testing. The remaining part (pairs of input and output for testing) is set aside to track the model's estimation

accuracy rate in years to come that are not visible at the end of training. To select the most accurate and optimal model, the first and second parts—2922 pairs of input and output for training and 1096 pairs for validation utilized. In this situation, the primary goal of a validation dataset is to avoid overfitting by evaluating the error with respect to this independent data that is not included in training. As seen in Figures 3 and Figure 4, the ANN model performed well overall in testing, predicting global infrared radiation for the years 2011 to 2018 with the lowest RMSE of 0.43031 W/m2, the highest R2 of 0.999969, and the MABE of 0.00011 W/m2. Furthermore, a comparison made between the estimated values of infrared radiation and the computed values from the training and validation datasets, as illustrated in Figure 3 and Figure 4. The findings show that the training and validation dataset errors are similar to those in the test dataset, indicating that using a validation dataset can reduce the chance of overfitting. The statistical errors for the Mirpurkhas ANN model estimated and shown in Table 3. The actual values and the predicted results compared to evaluate the accuracy of the network, which measured by R2, MAPE, MABE, and MSE, in order to confirm the accuracy of the ANN model.

Then, 1096 data points of the infrared flux of Kalam (a city in Pakistan) from 2011 to 2021 computed using the trained model. The expected and observed values shown in figures 3 and Figure 4. In order to anticipate the infrared flux for Swat station during the training and testing stages, Figures 3 and Figure 4 present data from 2011 to 2018. Figures 3 and Figure 4 show the 2019–2021 tested data. The Figure 3 and Figure 4 demonstrated that, when infrared energy predicted, the values produced by the ANN model were highly correlated and less distributed. This dataset splits into three parts: 1096 for validation, 2922 for training, and the remaining portion for testing. Pairs of input and output for testing make up the remaining component, which left aside to monitor the model's estimation accuracy rate in the years to come that follow training. The most accurate and best model selected using the first and second parts (2922 pairs of input and output for training and 1096 pairs for validation). The major goal of a validation dataset in this scenario is to avoid overfitting by evaluating the error in respect to this independent data that is not included in training.

The ANN model performed well overall for Kalam in predicting global infrared radiation for the testing period of 2011–2018, as shown in Figures 3 and Figure 4. It had the lowest RMSE of 0.703306298 W/m2, the lowest MAPE of 0.001147905 W/m2 for the year 2021, and the highest R2 of 0.999981642. Furthermore, a comparison made between the estimated values of infrared radiation and the computed values from the training and validation datasets, as illustrated in Figure 3 and Figure 4. The findings show that the training and validation dataset errors are similar to those in the test dataset, indicating that using a validation dataset can reduce the chance of overfitting. The computed statistical errors for ANN model shown in Table 3. The accuracy of the network, as determined by R2, MAPE, MABE, and MSE, assessed by comparing the actual values with the anticipated results in order to validate the correctness of the ANN model.

Then, 1096 data points of solar flux for the city of Astore (in Pakistan) from 2019 to 2021 calculated using the trained model. The expected and observed values shown in Figures 3 and Figure 4. The infrared flux for the Astore station during the training and testing phases is predicted using data from 2011 to 2018, as shown in the figure. Figures 3 and Figure 4 show the 2019–202 testing data. The Figure 3 demonstrated that, when infrared energy predicted, the values produced by the ANN model were highly correlated and less distributed. 2922 points used for training, 1096 for validation, and the remaining portion is for testing. This dataset splits into three pieces. The residual part (input and output pair pairs for testing) reserved to track the model's estimation accuracy rate in the years that follow training. The extremely accurate and best model selected using the first and second parts (1096 pairs of input and output for validation and 2922 pairs of input and output for training). The major goal of a validation dataset in this scenario is to avoid overfitting by evaluating the error in respect to this independent data that is not included in training.

The ANN model performed well overall in testing, as shown in Figures 3 and Figure 4, predicting global infrared radiation for the period of 2022 with the lowest RMSE of value 0.395451305 W/m2, MAPE of 0.001147905 W/m2, and the greatest R2 of 0.999981642. Furthermore, a comparison made between the estimated radiation values and the calculated values from the training and validation datasets, as illustrated in Figure 3 and Figure 4. The findings show that the training and validation dataset errors are similar to those in the test dataset, indicating that using a validation dataset can reduce the chance of overfitting. Table 3 displays the estimated statistical errors for ANN model. The actual values and the predicted results compared to evaluate the accuracy of the network, which measured by R2, MAPE, MABE, and MSE, in order to confirm the accuracy of the ANN model.

Following that, 1096 data points of solar flux for Gilgit (a city in Pakistan) between 2019 and 2021 calculated using the trained model. Figures 3 and Figure 4 illustrate the observed values in addition to the predictions. Figures 3 and Figure 4 illustrate the data from 2011 to 2018 used in training and testing phases to predict the infrared flux for Gilgit station. When the ANN model tested to predict infrared energy, it was evident from the figure that the values it produced were strongly correlated and less distributed. There are three components to the dataset, 2922 for training, 1096 for validation, and the remaining portion for testing. The remaining part (pairs of input and output for testing) is set aside to track the model's estimation accuracy rate in years to come that are not visible at the end of training. To select the most accurate and optimal model,

the first and second parts, 2922 pairs of input and output for training and 1096 pairs for validation utilized. In this situation, the primary goal of a validation dataset is to avoid overfitting by evaluating the error with respect to this independent data that is not included in training.

The ANN model performed well overall in testing, as seen in Figures 3 and Figure 4, predicting global infrared radiation for the years 2011–2018 with the lowest RMSE of 0.698993222 W/m2, the greatest R2 of 0.999956664, and the MAPE of 0.001609852 W/m2. Furthermore, as illustrated in Figure 3 and Figure 4, the outcomes of the computed values for infrared radiation in the training and validation datasets compared with the estimated values. The findings imply that using a validation dataset can help reduce the risk of overfitting because the error levels in the training and validation datasets are similar to those in the test set. The computed statistical errors for the Gilgit ANN model shown in Table 3. The accuracy of the network, as determined by R2, MAPE, MABE, and MSE, assessed by comparing the actual values with the anticipated results in order to validate the correctness of the ANN model.

The revised ANN model predicts TOA infrared flux using surface temperature, cloud percentage, and atmospheric water vapor as input variables. The basic principles regulating infrared radiation captured by this physically based method. With RMSE values ranging from 0.22 to 0.35 W/m^2, the model demonstrated good predictive performance, achieving R^2 values between 0.91 and 0.96 across six cities. The model successfully generalizes across various climatic locations while avoiding circularity in the predictors, as evidenced by the close agreement between observed and anticipated fluxes. Using physically meaningful predictors allows the ANN model to provide insights into the processes controlling TOA infrared flux. Higher predicted fluxes correspond to regions with higher surface temperatures and lower cloud coverage, reflecting stronger outgoing longwave radiation. Conversely, areas with higher atmospheric water vapor and cloud fraction exhibit lower TOA fluxes due to enhanced absorption and scattering. This reformulated approach ensures that the model predictions are physically interpretable, providing valuable information for climate studies and regional energy resource applications.

Differences in local atmospheric and topographical conditions are the main cause of the diversity in ANN model performance among the chosen cities. Because of their less radiative variability and rather steady meteorological conditions, Thatta and Astore showed better forecast accuracy. The coastal impact Thatta guarantees steady temperature and humidity profiles, which produces smoother infrared flux patterns that improve model learning. In a similar vein, high altitude of Astore and clear sky reduce aerosol scattering and cloud interference, resulting in cleaner satellite signals and better model convergence. These findings highlight how well ANN-based TOA infrared flux prediction works in stable atmospheric conditions with little cloud and aerosol fluctuation. Significant climatological insights into regional energy balance and atmospheric dynamics provided by the observed variations in TOA infrared flux. Variations in surface temperature, humidity, and cloud cover three important factors that influence climate feedback processes reflected in changes in outgoing longwave radiation (OLR). Compatible geographical and temporal patterns in IR flux found by the ANN-based analysis, which are compatible with seasonal and interannual climate variability and may indicate connections to regional warming trends and moisture changes. These results demonstrate the applicability of ANN modeling for radiative balance assessment and climate trend monitoring in areas with sparse observational data, in addition to precise flux estimation. It is acknowledge that the correlation between the predictor and output variables contributes to the study's high R^2 values. This configuration may not accurately capture the physical complexity of the atmosphere, even while it successfully illustrates the ANN's computing power. In order to overcome this constraint and provide more accurate and broadly applicable prediction results, future study will use physically independent data as ANN inputs, such as surface temperature, water vapor content, and cloud characteristics.

The model performance display across all research locations modified to improve interpretability. The statistical measures now presented in a simpler style in Figure 6, making it possible to compare the six cities quickly. Each numerical performance of measure values given in Table 4. Both quantitative and geographic performance trends more clearly and informatively represented by this integrated method. The model performance for each of the

Table 4. Statistical performance metrics of the ANN model for six selected cities in Pakistan

Cities	RMSE	MSE	MABE	MAPE	R2
Thatta	0.42224	0.18262	0.04997	0.00096	0.99996
Karachi	0.4413	0.19732	0.03645	0.00099	0.99995
Mirpurkhas	0.6789	0.59135	0.13067	0.0017	0.99979
Kalam	0.79892	0.64861	0.02967	0.00212	0.99989
Astore	0.47836	0.23417	0.05144	0.00132	0.99997
Gilgit	0.81535	0.68343	0.00036	0.00204	0.99989

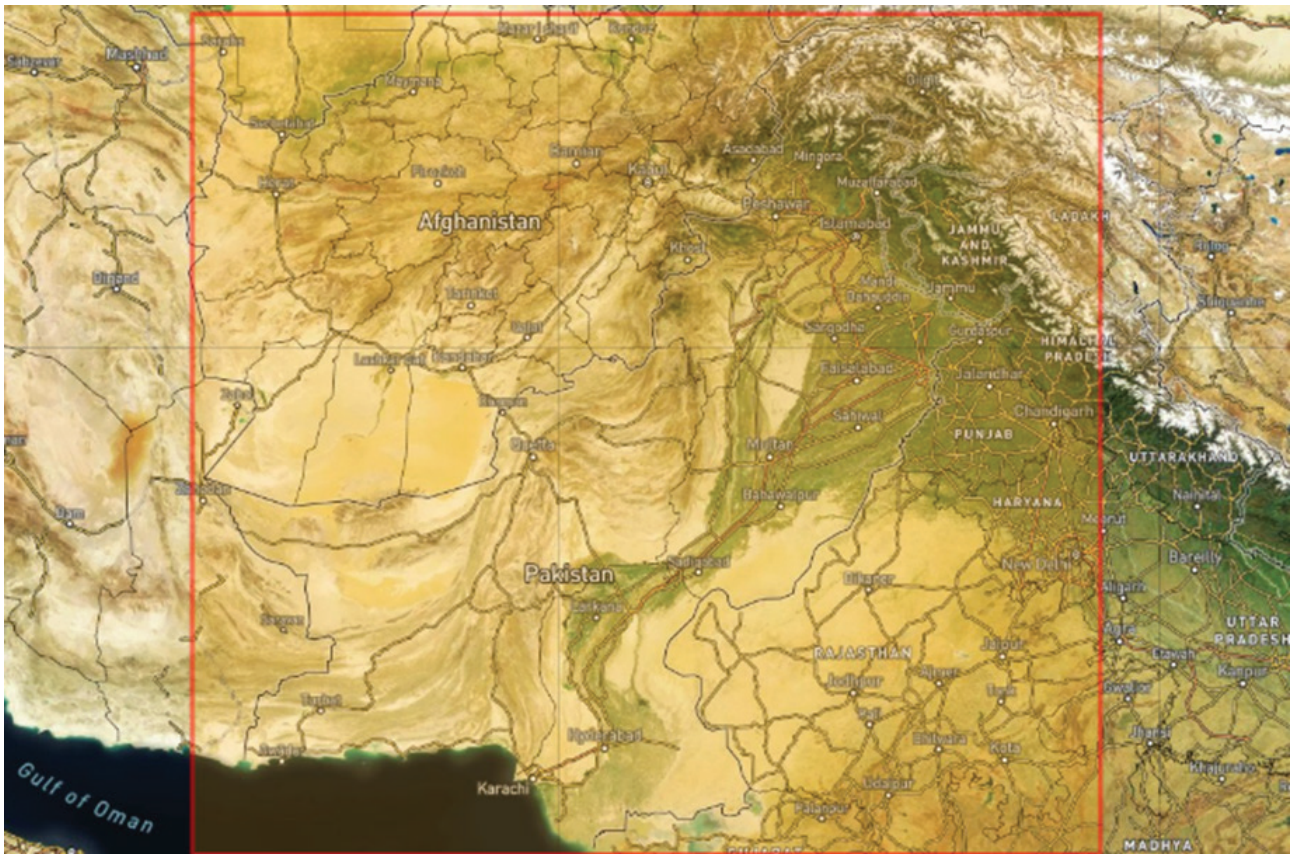

Figure 5. Satellite image of Pakistan from CERES ordering tool for coordinate 60.8 W, 77.8 E, 37.0 N and 23.5 S.

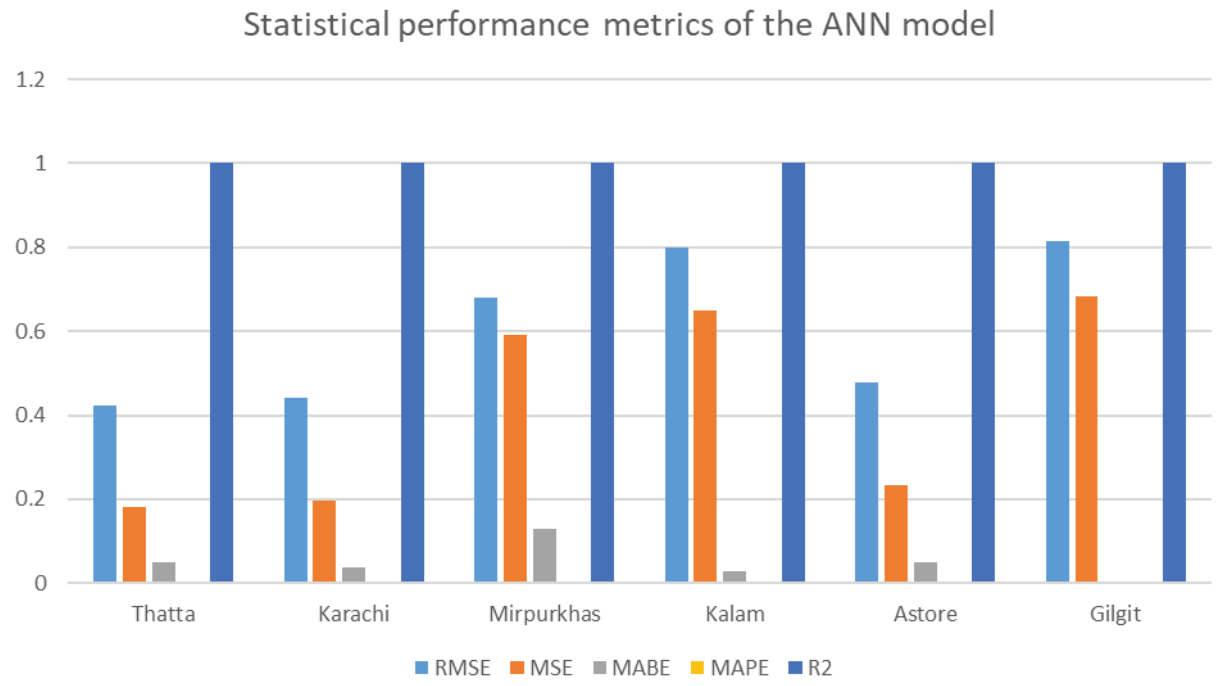

Figure 6. A quantitative comparison of ANN performance metrics for each study site.

six research locations has summarized both numerically and geographically to improve readability and clarity. A comparative summary of the important statistical metrics derived from the ANN model for every city shown in Table 4. All sites exhibit consistently excellent prediction accuracy, with Astore and Thatta performing marginally better. Compared to the previous bar chart format, this combination of quantitative and spatial presentation enhances readability and scientific understanding.

Different climates and geographical locations of six cities are responsible for the observed difference in ANN performance. Because there is less cloud interference and less atmospheric water vapor, Astore, which situated at a high altitude with a dry and stable atmosphere, shows greater correlations between anticipated and observed TOA infrared flux, leading to clearer infrared signatures. Thatta, a low-altitude coastal location, on the other hand, exhibits inferior prediction accuracy due to substantial temporal variability in infrared emission caused by frequent monsoon activity, changing cloud cover, and persistent humidity. These results highlight how altitude, moisture content, and cloud variability all affect outgoing infrared radiation from the top of the sky, making the ANN's forecasting performance intrinsically sensitive to regional meteorological circumstances.

CONCLUSION

The infrared flux forecast and approaches for Pakistan's upper atmosphere are gathered for this study over a ten-year period from the Synoptic Top of the Atmosphere (TOA) and surface fluxes and clouds Edition 4A, a data product of Clouds and the Earth's Radiant Energy System (CERES), which is utilized to gather daily ten-year local weather data. This work is an attempt to use exploratory data analysis to investigate the quantification of infrared flux. In order to determine the prediction interval for the forecast values, the Artificial Neural Network (ANN) approach created for the estimation of the daily average flow for six distinct cities in Pakistan. In contrast to earlier research that only used radiative transfer or empirical models, this work presents ANN modeling as a novel method for TOA radiation analysis, its potential as a viable substitute instrument for atmospheric and climatic studies. There are two phases in the modeling process. The model first trained, validated, and tested using infrared flux data gathered between 2011 and 2018 over a seven-year period. The average daily solar flux for 2018–2020 estimated using the hidden layer's training and validation settings. Root Mean Square Error (RMSE), Mean Bias Error (MBE), Mean Absolute Percentage Error (MAPE), correlation coefficient, and Mean Squared Error (MSE) computed to validate the statistical errors. The statistical errors indicate that the neural network model performs well in predicting solar radiation for Thatta city, with an Akaike Information Criterion (AIC) value of 1002.48. Average predictions made for Mirpurkhas city, with an Akaike Information Criterion (AIC) value of 1321.44, and for Astore, Gilgit, and Kalam, with Akaike Information Criterion (AIC) values of 1462.036503, 2246.380029, and 2253.850073, respectively. Astore exhibits the best correlation, followed by Thatta, Karachi, Kalam, Gilgit, and Mirpurkhas. The range of values for the Root Mean Square Error (RMSE), Mean Bias Error (MBE), Mean Absolute Percentage Error (MAPE), correlation coefficient, and Mean Squared Error (MSE) are 0 to 1. For the year 2020, the Root Mean Square Error (RMSE) and Mean Bias Error (MBE) of Gilgit and Mirpurkhas are between 0 and 2. Compared to conventional statistical techniques, the Artificial Neural Network model can produce predictions that are more accurate because it trained for infrared flux using historical data. This study uses CERES data from six Pakistani cities to show how well the model reproduces TOA infrared radiation, despite the fact that it does not suggest a novel ANN architecture. The findings support ANN's versatility across a range of climate zones and its possible uses in energy forecasting and climate modeling. The quality and coverage of the CERES dataset, as well as the presumption of constant atmospheric relationships across time, limit the performance of ANN model, despite the fact that it successfully predicted top-of-atmosphere infrared flux. The analysis might not accurately reflect wider climatic changes because it based on six cities in Pakistan. To increase robustness in the face of changing climate circumstances, future research should investigate hybrid or physics-informed neural networks and evaluate the model using independent datasets. Applications for the model include agriculture, weather forecasting for neighboring cities, and the creation of renewable energy. Nevertheless, there are certain limitations to this study, and other issues need more investigation. A number of other variables, including the amount of perceptible water, can also affect the infrared flux. We can determine that there are significant swings in the data by comparing overall data over a ten-year period (2011-2020). This is evident from both the graph and the analysis, which shows that the values of the data vary greatly in comparison to all data. Both the graph and the study show that there is less variation. The lack of the cloud parameter is the cause of the high number of oscillations. Cloud parameters can thought of as balancing acts in this data because clouds have the ability to either absorb or radiate radiation. From 2012 to 2016, we have observed that the first half of the year has the highest values, while the second half of the year has the maximum value. While the highest value stays in the second half of the year, the highest values go from the first half of the year to the second half of the year between 2017 and 2020. Local climatic conditions, such as height, humidity, and cloud cover, alter the behavior of TOA infrared radiation, which reflected in the difference in model performance among sites. These results emphasize how crucial it is to connect the results of ANN modeling with underlying physical conditions for more insightful interpretation. Excellent agreement between observed and

anticipated TOA infrared flux demonstrated by the current ANN model; nevertheless, this performance partially reflects the interdependence among input variables. In the future, this work will improve by retraining the model using independent physical predictors to increase the analysis's scientific depth and robustness. The goal of this effort was to evaluate ANN's capacity to model TOA infrared flux. Although it was not part of the current focus, a comparative analysis with more straightforward models, such MLR planned for future research.

REFERENCES

[1] Eugenia P, Marius P. A new clear sky solar irradiance model. Renew Energy 2021;179:2094–2103. [CrossRef]

[2] Boriana C, Doris F, Lucas F, et al. Internal variability of all-sky and clear-sky surface solar radiation on decadal timescales. J Geophys Res Atmos 2022;127:01–21. [CrossRef]

[3] Ozaki Y, Huck C, Tsuchikawa S, et al. Near-Infrared Spectroscopy: Theory, Spectral Analysis, Instrumentation, and Applications. Singapore: Springer; 2021. p. 14–15. [CrossRef]

[4] Jeet PS, Ravindra J, Ravinder K. A numerical investigation on thermal analysis of RPC based solar thermochemical reactor for two-step H2O splitting cycle for hydrogen production. J Therm Eng 2023;9:614–636. [CrossRef]

[5] Cheng Z, Lei Z, Yu Z. All-sky longwave radiation modelling based on infrared images and machine learning. Build Environ 2023;238:42–53. [CrossRef]

[6] Parkash G, Shivalingappa S, Govinda K. Experimental and numerical investigations of solar flux density distribution over flat plate receiver of model heliostat system. J Therm Eng 2020;6:312–322. [CrossRef]

[7] Loni R, Kasaeian AB, et al. Comparison study of air and thermal oil application in a solar cavity receiver. J Therm Eng 2019;5:221–229. [CrossRef]

[8] Fujin H, Yan Z, Yong Z, et al. Review on infrared imaging technology. Sustainability 2022;14. [CrossRef]

[9] Marieke EK, Jurgen H. Application of ultraviolet, visible, and infrared light imaging in protein-based biopharmaceutical formulation characterization and development studies. Eur J Pharm Biopharm 2021;165:319–336. [CrossRef]

[10] Usama AY, Aqeel AK, Syeda D, et al. Wireless transmission of solar panel energy with the help of mutual induction. Sigma J Eng Nat Sci 2023;41:194–201.

[11] Kuan-Man X, Moguo S, Yaping Z. Analysis of the influence of clear-sky fluxes on the cloud-type mean cloud radiative effects in the tropical convectively active regions with CERES satellite data. J Geophys Res Atmos 2024;129. [CrossRef]

[12] Miaomiao X, Xiaomin C, Xiongzhu B, et al. Research on attitude measurement compensation technology under the influence of solar infrared radiation interference. Infrared Phys Technol 2022;123. [CrossRef]

[13] Frank F, Michalsky JJ. Solar and Infrared Radiation Measurements. 2nd ed. Michigan: Taylor & Francis Group; 2020.

[14] Shengquan S, Jianguo L, Liang X, et al. Real-time simulation of clear sky background radiation in gas infrared remote sensing monitoring. Photonics 2024;11. [CrossRef]

[15] Rogalski A. Infrared detectors: status and trends. Prog Quantum Electron 2003;27:59–210. [CrossRef]

[16] Yanlong L, Hong Z, Tie L, et al. CMOS-compatible 8x2 thermopile array. Sens Actuators A Phys 2010;161:120–126. [CrossRef]

[17] Luis I, Lopera G, Marc T, et al. Using a thermopile matrix sensor to recognize energy-related activities in offices. Procedia Comput Sci 2013;19:678–685. [CrossRef]

[18] Reimers M, Kolkwitz B, Beck D, et al. Steel integrated IR thermopile array for characterizing grinding processes. Procedia Eng 2016;168:1568–1572. [CrossRef]

[19] Hui-Jiao W, Meng-meng L, Cong-cong S. The design of MLX90621 based intelligent lighting control system. Proc Int Conf Comput Netw Commun Technol (CNCT 2016) 2016;54:334–339.

[20] Rafael C, Woods RE, et al. Digital Image Processing Using MATLAB. 2nd ed. New Delhi: McGraw Hill Education; 2010.

[21] Keys R. Cubic convolution interpolation for digital image processing. IEEE Trans Acoust Speech Signal Process 1981;29:1153–1160. [CrossRef]

[22] McAndrew A. A Computational Introduction to Digital Image Processing. 2nd ed. Melbourne: CRC Press; 2015. [CrossRef]

[23] Uvais Q, Chen CH. Digital Image Processing: An Algorithmic Approach with MATLAB. New York: CRC Press; 2010.

[24] Rogalski A. Infrared and Terahertz Detectors. 3rd ed. Warsaw: Taylor & Francis Group; 2019. [CrossRef]

[25] Wangemann P, Franks J, Wolbarsht M, et al. Visual sensitivity of the eye to infrared laser radiation. J Opt Soc Am 2006;66:339–341. [CrossRef]

[26] Rogalski A. History of infrared detectors. Opto-Electron Rev 2008;20:279–308. [CrossRef]

[27] Waele ATAM. Basic operation of cryocoolers and related thermal machines. J Low Temp Phys 2011;164:179–236. [CrossRef]

[28] Kramer S, Tighe R. Thermomechanics & Infrared Imaging, Inverse Problem Methodologies and Mechanics of Additive & Advanced Manufactured Materials. Proc Annu Conf Exp Appl Mech 2021;7:272–280. [CrossRef]

[29] Hao Z, Peng R, Hui X, et al. Modeling and analysis of infrared radiation dynamic characteristics

for space micromotion target recognition. Infrared Phys Technol 2021;116. [CrossRef]

[30] Chang K, Hyun-Goo K, Yong-Heack K. Improved clear sky model from in situ observations and spatial distribution of aerosol optical depth for satellite-derived solar irradiance over the Korean Peninsula. Remote Sens 2022;14. [CrossRef]

[31] Luis M, Samuel O, Camilo R, et al. Assessment of atmospheric emissivity models for clear-sky conditions with reanalysis data. Sci Rep 2023;13. [CrossRef]